JMATPRO	Journal of Advanced Materials and Processing 9 (3): 23-34, Summer 2021 http://jmatpro.iaun.ac.ir 20.1001.1.2322388.2021.9.3.2.2

Research Paper

The Effect of Reverse Pulse Plating and Lanthanum Addition in Plating Bath on Corrosion Resistance of Austenitic Steel in Chlorine Solution

Leila Bakhtiari[1], Abdolhamid Jafari[2*], Shahriyar Sharafi[3]

1. Ph.D. student, Materials Science and Engineering Dept., Shahid Bahonar University, Jomhori-e-Eslami Blvd., Kerman, Iran

2. Associate Professor, Materials Science and Engineering Dept., Shahid Bahonar University, Jomhori-e-Eslami Blvd., Kerman, Iran

3. Professor, Materials Science and Engineering Dept., Shahid Bahonar University, Jomhori-e-Eslami Blvd., Kerman, Iran

ARTICLE INFO

Article history:

Received 10 November 2020
Accepted 16 December 2020
Available online 1 May 2021

Keywords:
Coating
Stainless steel
Lanthanum
Pulse reverse plating
Corrosion

ABSTRACT

The 316L nickel-chrome molybdenum austenitic stainless steel is commonly employed in various industries. This type of steel is particularly of interest in chemical industries, especially in harsh and corrosive environmental conditions. Although 316L stainless steel has good mechanical and corrosive characteristics, it fails to perform well in chlorine-containing aqueous environments. To overcome this issue, a Ni-La-Cr-Fe layer is applied to the 316L steel using the electroplating method. In addition, the reverse pulse plating method is used to control the ion deposition kinetics. The plating current application duration (on-time), the current disruption duration (off-time), and (TRev) are the control parameters of the duration and polarity of the pulse. Finally, the coated layer acquires an average thickness of 6.83 after applying on-time and off-time repeatedly and performing SEM and polarization tests in 1.5% solution at 50 Celcius degrees. Furthermore, the desired surface morphology is achieved, and corrosion resistance is 160 times higher than 316 bare steel. Applying the reverse pulse plating method, adding beneficial compounds of saccharin and SDS, and using lanthanum chloride in the plating bath are the essential reasons to successfully add a coating layer on the 316 bare steel.

Citation: Bakhtiari, L., Jafari, A., Sharafi, Sh., (2021) The Effect of Reverse Pulse Plating and Lanthanum Addition in Plating Bath on Corrosion Resistance of Austenitic Steel in Chlorine Solution, Journal of Advanced Materials and Processing, 9 (3), 23-34. Dor: 20.1001.1.2322388.2021.9.3.2.2

[*] **Corresponding Author**:
E-mail: jafham2020@gmail.com

1. Introduction

The SS316L nickel-based stainless steel is less prone to intergranular corrosion than SS316 steel due to its lower carbon contents. Plate heat exchangers are usually made of SS316L steel. Despite the appropriate corrosion properties of this kind of steel, it suffers from local corrosion. This kind of corrosion possibly stems from the water-soluble industrial salt flowing among the plates. Therefore, numerous studies are conducted on the effects of chlorine ion, which is one of the most crucial ions in cavitation and local corrosion. A combination of water, heat, and chloride-containing salt causes pitting corrosion of the stainless steel. Surface contamination by hygroscopic salt can result in very deep pits over several months. When corrosion occurs under thin moisture layers, pit extension results in shallow pits [1]. The primary reason for chloride influence is attributed to the behavior of passive film on stainless steel in wet and atmospheric conditions. Numerous studies on the effects of environmental variables on the corrosion resistance of stainless steel against pitting corrosion in the presence of chloride demonstrated an inverse linear dependence of the corrosion potential on the temperature in the 25~100ºC interval. Therefore, E_{pit} decreases as the temperature is raised. When the temperature is risen from 25°C to 88°C, the potential decreases four times. The temperature effect on the morphology of the pits in such environments becomes more noticeable at higher temperatures, and shallow spread ones at higher temperatures replace the deep localized pits at temperatures lower than 150°C [1-4].

The density of the pits is inversely dependent on the temperature. In addition, the number of pits decreases at temperatures higher than 100°C, while their diameters are increased [5]. The relationship between the chloride concentration and corrosion resistance in stainless steel is investigated. The studies revealed that the pitting tendency is reduced due to higher positive potentials at lower levels of concentration. In fact, the threshold temperature and amount of chloride for the pitting to have a steady-state corrosion form are shown to be 50°C and 0.5 mol, respectively [5-9]. Heat-resistant steels are used in heat exchangers due to their appropriate mechanical properties and corrosion resistance that is characterized by the composition change of the surface steel [10-13]. A continuous dense coating prevents the diffusion of anions into the alloys. Therefore, generating these kinds of coating naturally or technically on the surfaces is the key to the corrosion resistance of an alloy. Researches demonstrated that the Reverse Pulse Electroplating (RPE) method is influential in forming composite layers and high entropy alloys that are dense and stable and present excellent corrosion resistance [14-17]. Pulse Plating (PP) is used to form a wide range of compositions and properties through effective alteration of the catholyte/cathode interfaces [18-20]. The effects of the rare earth elements on the corrosion (particularly pitting corrosion) and high-temperature oxidation of steels (due to their unique electronic structures and chemical activity) are reported [21-26]. Rare earth salt can improve the Throwing Power (TP) of a plating solution, reduce the grain size of the plating alloy, and make the microstructure of the coating more uniform [27-31]. Electrochemical Impedance Spectroscopy (EIS) is often used to characterize the quality of barrier coating systems. The EIS response is stable, and Kramers-Kronig consistency requirements are met when the three parameters of saturated water volume fraction of the coating, diffusion rate, and the electrical response are low. Higher rates of diffusion, water volume fractions, or electrical impedance responses to the composite system can influence the resonance frequency and consequently the relative impact on the real and imaginary parts of the coating impedance [32]. High hardnesses and a slight increase in corrosion resistance are studied and reported by applying Direct Current Plating (DCP) methods or conventional pulsed plating methods [27-30]. The latter is achieved by including some rare earth metals in nickel plating baths for mild steel. However, according to this study, no research has been conducted on enhancing mechanical performance and high-temperature corrosion by combining lanthanum with the RPE technique.

2. Experiments

2.1. Materials and Research Methods

It is demonstrated in this research that the best possible way to increase the corrosion resistance of 316L steel is to use the Pulsed Electroplating (PE) method and rare earth elements in the plating bath (according to the articles in the field [18-28]. Lanthanum is selected among the rare earth elements because of its results in previous researches [28,29]. In all previous studies, the bath-plating method consists of rare-earth elements, direct-flow plating, or pulsed plating. During the almost three-year period of this study, none of these two methods are shown to be suitable. Finally, the experiments continue until reaching the surface since the produced coating by the reverse pulse plating (RPP) method has a finer grain size, more density than the PP and Direct Flow (DF) methods, and higher quality. The RPP method is applied in this regard [33, 34]. The first thing to be noted in the case of plating ranges is that the TOff is selected in every plating time if the off-time (TOff) is greater than on-time (Ton) since the unstable buds and impurities have more time to peel off the surface, leading to better coating quality, compression, and

adhesion. Multiple TOn and TOff times are tested for the three ranges listed in Table 3. Finally, the best results among all of the tested times are listed. It is observed that range 1 satisfies the objective of the present study among the three ranges.

Experiments are performed using double distilled-deionized water. 3.5% NaCl is added to the water, so the specimens are tested without a calcareous scale on the surface. The SS316L stainless steel specimens of Table 1 are polished with 2000 abrasive papers with one side coated by a thermoset resin.

Table 1. Elemental analysis of SS 316 L austenitic stainless steel

Element	C	Si	S	P	Mn	Ni
Quantity (%)	0.018	0.70	0.002	0.03	1.17	10.22
Element	Cr	Mo	Fe	Cu	W	Co
Quantity (%)	16.71	2.03	68.5	0.36	0.02	0.18

The plating anode is made of 99.9% nickel, and the constituents of the electroplating bath are all Merck's laboratory-grade reagents, as shown in Table 2. Table 3 summarizes various electrical pulse ranges used for the electroplating process.

Table 2. Chemical composition of Ni-La-Cr-Fe plating bath

Constituents	Concentration (gL^{-1})
$NiSO_4.6H_2O$	250
H_3BO_3	35
$C_{12}H_{25}SO_4Na$	0.35
Saccharin	1
$Na_3C_6H_2O.2H_2O$	60
AlCl3.6H20	100
CrNO3.6H2O	100
$LaCl_3.7H_2O$	1
Plating Parameters	
Current Type	Pulse
Plating Time (min)	40
Temperature ($^{\circ}C$)	40
Current Density (Acm^{-2})	1

Table 3. Pulsing ranges employed for Ni-La-Cr-Fe layer plating

No.	On-Time (TOn) /µs	Off-Time (TOff) /µs	Reverse Pulse Time (TRev) /µs
range-1	400	700	100
range-2	1000	1000	100
range-3	10000	10000	100

Fig. 1 shows the represented pulse sequence of table 3 graphically. The current density and TRev are selected to be 1 Acm^{-2} and 100µs, respectively. These values ensure that a fine grain structure and smooth morphology are used throughout the experiment. The plating bath contains $0.35gL^{-1}$ of $C_{12}H_{25}SO_4Na$ to raise the over-potential of the hydrogen evolution reaction (HER). This, in turn, cuts hydrogen produced at cathodic points, eliminates the embrittlement and pinhole formation, and consequently improves coating integrity.

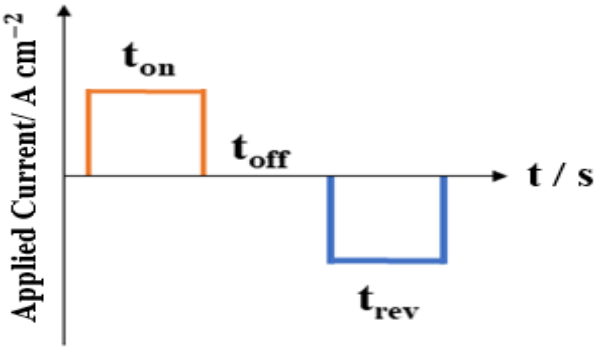

Fig. 1. Schematic representation of PRP plating range used in this study.

2.2. Characterization Method

The XRD, SEM, Potentio-dynamic polarization experiments are performed to characterize the structure and corrosion properties. Moreover, the Tofel polarization is performed at a scan rate of 1mVS-1 using Model PARSTAT-2273 EG&G potentiostat with saturated Ag/AgCl and Pt gauze as a reference and a counter electrode, respectively. The potentials of the electroplated specimens are allowed to stabilize in a 3.5wt% NaCl solution in the potentiostat's three-electrode cells for one hour before each test. The tests are also repeated three times to ensure reproducibility, and the results are analyzed using the Powersuite software. The elemental composition of the compounds formed on the surface and crystallography and morphology of the constituents are studied using SEM Model TeScan Mira III, with EDS for point and linear element analysis and element-distribution mapping. The X-Ray Diffraction (XRD) technique is implemented using Philips Xpert and Cu-kα radiation to evaluate the phase patterns.

3. Results and Discussion

The XRD results of lanthanum-doped coatings for Ni_3La_7, NiFe, and CrFeNi are shown in Fig. 2. Ni_3La_7 indicates a well-developed crystalline structure and clearly demonstrates the coating's preferred growth for 200 planes. Its peak has an intensity three times greater than that of (020) and (022) planes that are the characteristics of nickel. As a rule, the sharp XRD peaks indicate a well-developed polycrystalline structure, and the low, wide peaks obtained from range-1 coatings (represented in Table3) confirm the microstructure is fine. Therefore, these peaks become wider and shorter in range-1 sample as the conditions tend to promote finer grains. This is validated by the SEM images represented in Fig. 3.

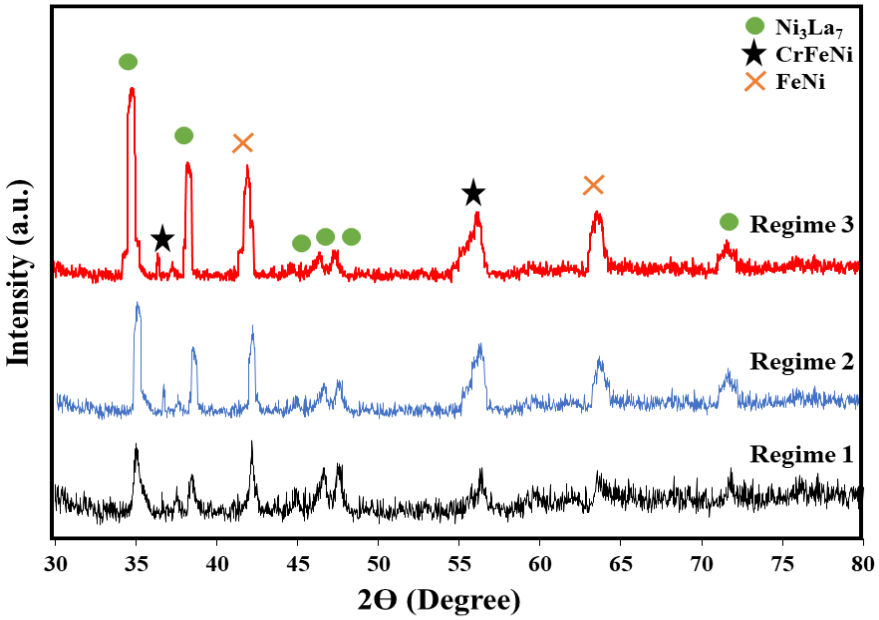

Fig. 2. XRD patterns of coatings formed under plating ranges 1, 2, and 3 of Table 3

The morphology of the specimen coated under the range-1 plating is shown in SEM pictures in Fig. 3. A uniform refined grain structure is often associated with enhanced mechanical properties and better

corrosion resistance, as demonstrated in Fig. 3. This culminates in directional deposit colonies comprising smaller spherical sub-sets. The range-1 samples are composed of closely packed 200nm spheres forming a homogenous surface. In contrast, range-2 samples have grains that clump together, forming coarse granules. This issue is more significant in range-3 coatings where tubular structures with diameters more than 500nm are produced. Some researchers observed this phenomenon and attributed it to the dominant effect of plating current [25]. However, this could be mainly true in DC or one-sided pulse plating, as shown later in this paper.

Rare-earth metals are posited with effects on the electrochemical depositing process and grain refining ability [21]. Lanthanum is a surface-active element with a large atomic radius of 0.1877nm and a valence state of La^{3+} [21, 26]. Thus, its outermost electron-deficient orbital is believed to cause physical adsorption on the surface of a cathode alongside any other cation. However, Ni^{2+} must be chemisorbed first on the basis of its overwhelming activity. Therefore, the nickel content of the electric double-layer falls, leading to a slight positive charge imbalance as La^{3+} concentration increases [26-28]. A rise in cathodic potential is required to provide the necessary energy reduction by deposition current that controls both the supply and subsequent reduction of Ni^{2+} and consequently, prevent the mentioned issue through migration of new cations [29]. It is discussed that a higher over-potential needed for nickel reduction helps to refine grains as the nucleation is sped up and the growth is reduced [28-30]. However, this mechanism is inadequate to explain the significant variation in the grain size in this work. Furthermore, the directional growth patterns observed as the PRP parameters are altered without changing the plating current. In contrast, the plating current frequency of on/off times is found to be particularly relevant. Compared with the effect of this parameter, the range-1 specimens with a shorter current-on time of 400 s (that is almost 2.5 times lower than that for range-2) acquire the most structural uniformity. This is due to the fact that this off-time prevents fast grain growth. The same holds for their current-off time of 700 s, which is enough to initiate nucleation. This time interval is enough to avoid the diffusion layer being formed on the cathode surface with undesirable concentration polarization effects. Finally, this research revealed that the ratio of "off" and "on" periods effectively achieves the desired metallurgical properties. A 2:1 ratio for samples formed under range-1 prevents excessive grain growth. However, as it tends to unity, both nucleation and growth patterns become irregular as this specific PRP function fails. The reverse current step decelerates deposition during the PRP process by removing some of the nascent nuclei. Therefore, according to the present study, it has to be kept within a tight range that falls within the 100~200 ms. Similar time ranges are suggested by other researchers [25]. This helps remove the boundary layer formed due to the diffusion of ions from the solution to the interface of a specimen without affecting the nucleation inordinately.

The linear cross-sectional scan shown in Fig. 4 (a) demonstrates that nickel is the dominant coating element considered for both the plating bath and the substrate containing Ni. It also demonstrates outwards declining concentration of iron that is only a constituent of the substrate, which contains nearly 68.5% Fe as shown in tables 1 and 2. This is in contrast to the observed behavior of nickel. The mechanism of alloy formation during plating by employing the modified nickel bath with appropriate additives is to first remove a thin layer of the stainless steel so that the constituents are incorporated in the converted surface layer. The film's iron content concentration is translated from the substrate towards the top of the coating. This confirms the source of the iron. It is accomplished by controlling the gradual diminishing concentration of Fe through the PRP parameters. Therefore, the common problem of separate phase forming that could jeopardize coating adhesion is tackled. Similarly, chromium is mainly concentrated around the substrate. It originates from this region and participates in forming quaternary Ni-Fe-Cr-Ta high entropy alloy. It also contributes to the coating's good corrosion resistance [31, 35]. The reverse pulse technique allows the dissolution of the nascent nuclei. It also provides conditions similar to the conversion coating (coupled with electroplating) and the Toff duration that prevents the diffusion layer from being generated. Fig. 4 represents the EDS linear scanning to analyze 30 points elementally starting from below the interface to the top of the coating. If the concentration of the main elements Fe, Cr, Ni at the interface is the same as those represented in Table 1, the conversion nature of the coating layer on 316 L steel is confirmed. These values are 73 wt.%, ~17 wt.%, and 9 wt.% for iron, chromium, and nickel, respectively, and shift towards those in the plating bath composition at distances away from the interface. The concentration profiles are produced inside the coating with clear inflection points. It is noteworthy that the inflection points in the three concentration profiles correspond to the same distances from the interface. This is due to the interactions between these elements when they dissolve in the substrate and fill holes in the

conversion/plated coating. The iron content is decreased rapidly so that the concentration at the inflection point drops by three times to 20 wt.%. In contrast, Ni content is increased to reach 8 the value of 0 wt.%. Chromium also follows a similar pattern and, at its inflection point, reaches almost 0.2 wt.%. The study on Cr as an alloying element during the PP approach revealed the need for high currents to enable Cr deposition [36-40]. The current off-time to on-time ratio and the current off-time is not constant, while our work's current density is constant. It is demonstrated that the controlling role of the current could be replaced by that ratio and the current off times. If there is no cathodic current, an acidic bath with surfactant additions can attack the substrate. Range-1 samples with the off-time to the on-time ratio of 2 show a tendency for restrained dissolution of Fe and Cr from the substrate at a constant reserve time. As explained before, it leads to moderate grain growth without hindering nucleation. The mentioned ratio for ranges 2 and 3 tends to unity with noticeable high Cr content extending further inside the coating due to long current-off time. Extremely long current-off times of nearly 10ms (e.g., in range-3) enable the electrolyte to attack and dissolve the constituents.

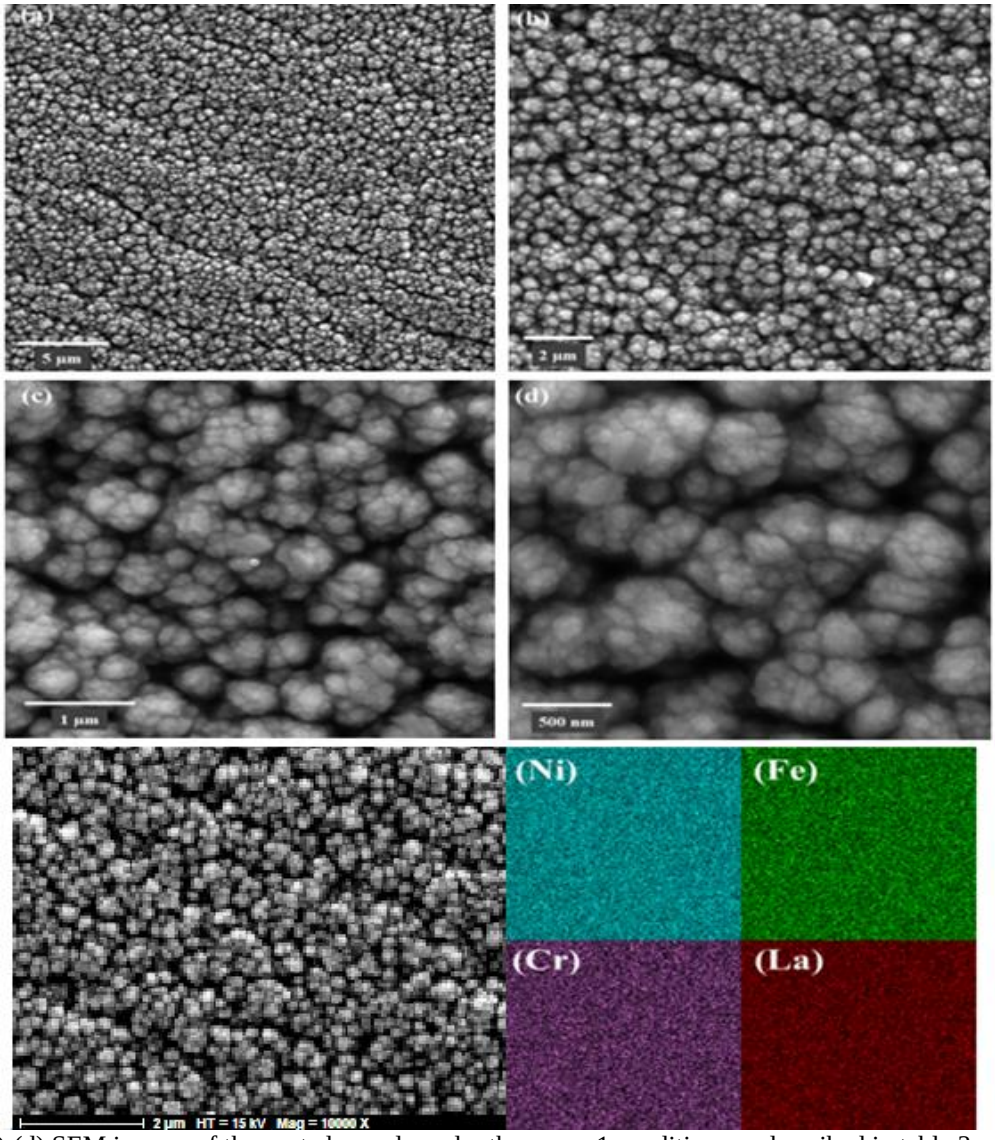

Fig. 3. (a)-(d) SEM images of the coated sample under the range-1 conditions as described in table 3, and (e) the uniformity of element distribution shown in the mapping of the same range

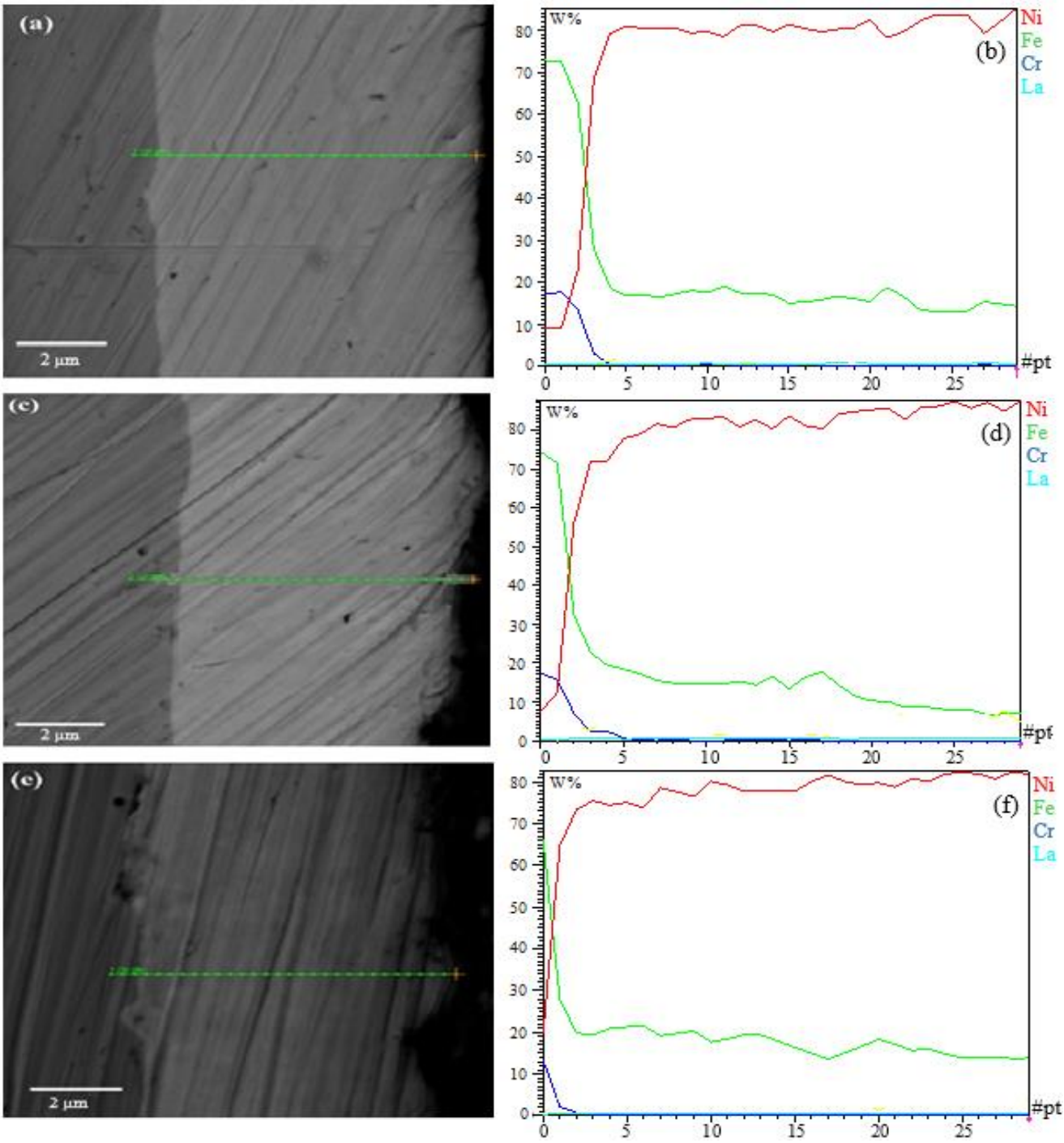

Fig. 4. SEM images of plated coating and the elemental linear scan analysis of the coating thickness. (a) and (b) are samples from range-1, (c) and (d) are samples from range-2, and (e) and (f) are samples from range-3

The experimental conditions, additives such as $LaCl_3.7H_2O$, and complexing agents positively shift the potential of the transition ions and depress the co-deposition of rare-earth elements that affect the deposition mechanism of the coating [28]. SEM images in Fig. 5 reveal that the coating thickness in the three samples created under the ranges 1, 2, and 3 are 6.83, 5.83, and 7.09µm, respectively. The interface of samples formed under range-1 shows no discontinuity and porosity. Therefore, the interface attains excellent adhesion. The range-2 samples demonstrate an acceptable coating quality but less adhesion and cohesion. However, samples of the range-3 plating suffer from a lack of cohesion and adhesion, with a noticeable porosity-filled coating interface. This reflects the poor corrosion performance, particularly when compared with bare SS316L.

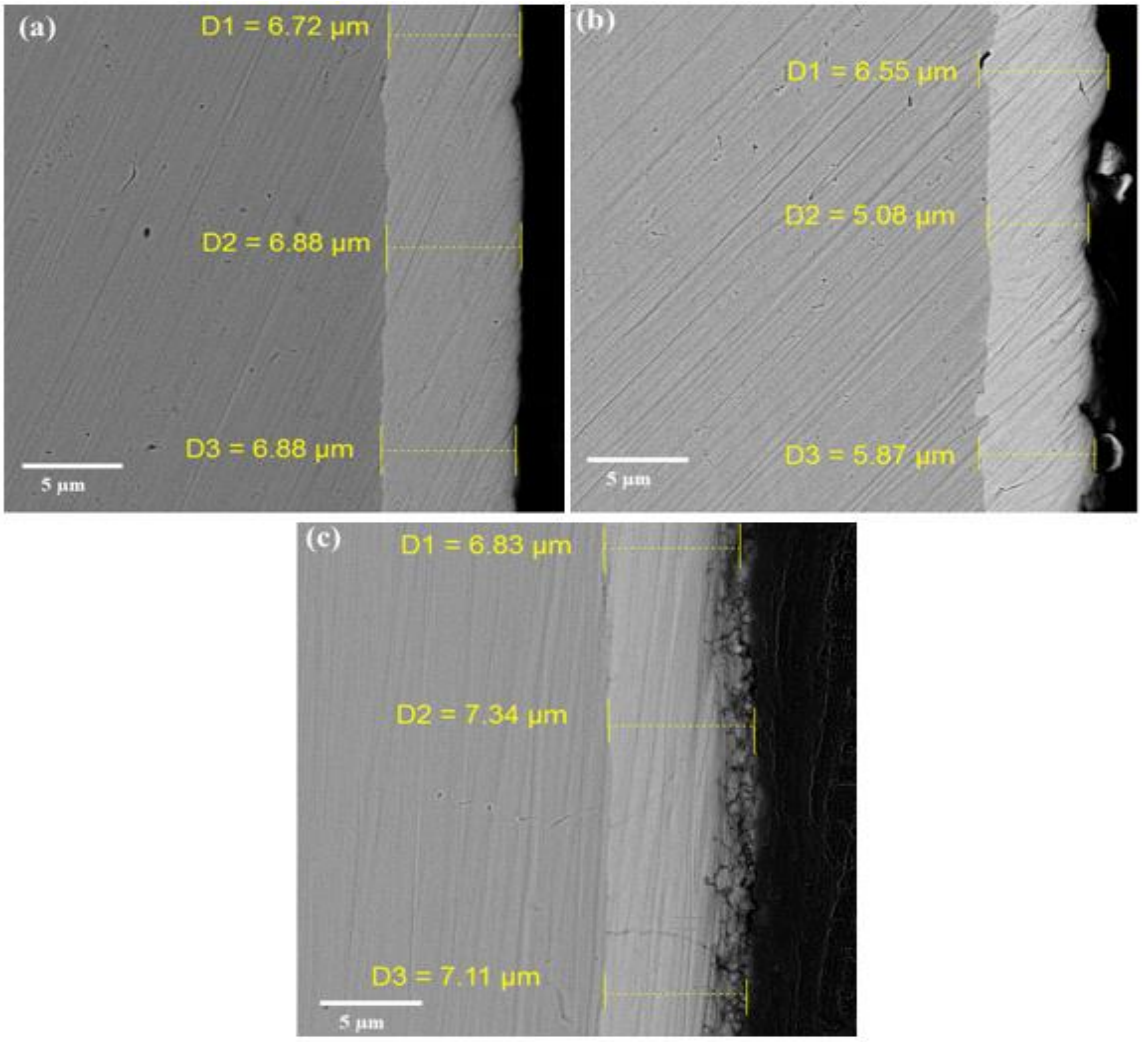

Fig. 5. SEM images of the cross-sections of the coating for samples created under (a) range-1, (b) range-2, and (c) range-3

The Tafel plots of the uncoated and plated sample 1 are shown in Fig. 6, and the numerical results of the polarization curves in Fig. 6 are shown in Table 4. The corrosion currents of the range-1 coated specimen are decreased compared with the bare SS316 indicating an improved resistance to corrosion. The comparative bar chart shown in Fig. 7 contrasts the corrosion current of these samples. It illustrates that the range-1 confers the highest corrosion resistance reducing the corrosion rate by almost 160 times compared to an uncoated sample. The overall improvement in corrosion resistance is attributed to the surface integrity of the passive layer due to chromium oxide formation, surface texture, and grain structure of the coating.

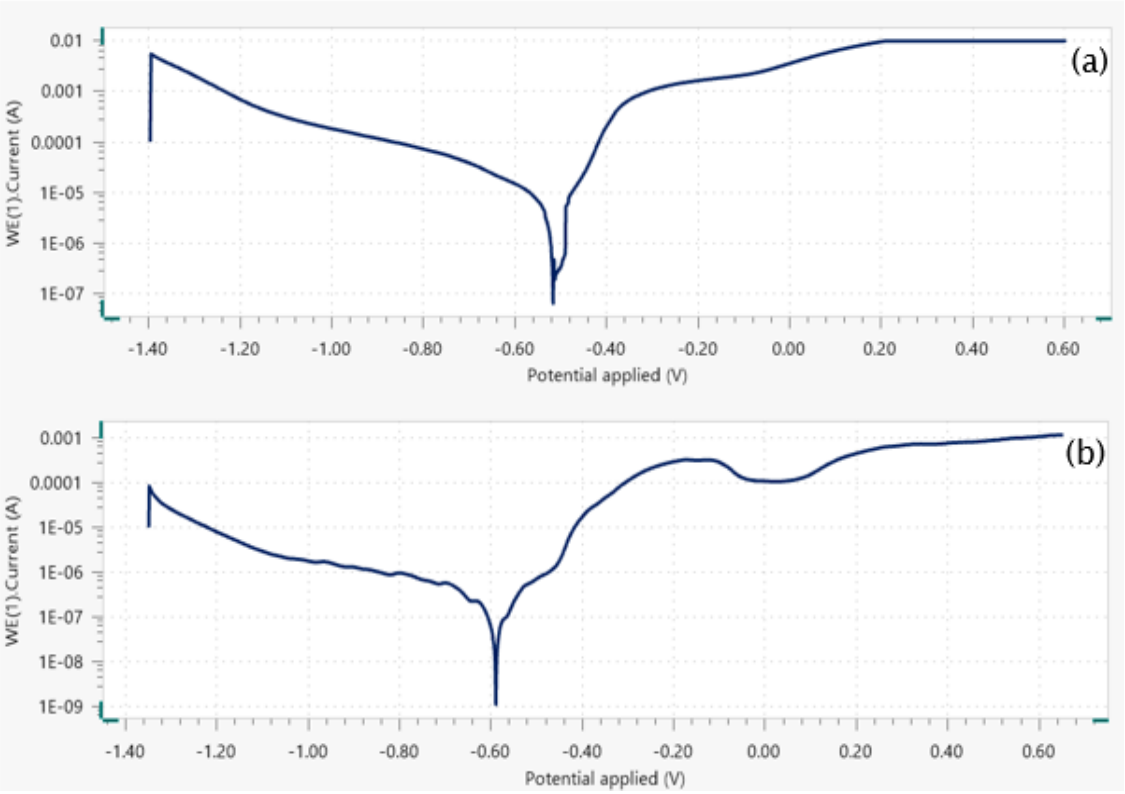

Fig. 6. Polarization diagrams of (a) 316 L steel without coating and (b) coated sample according to range-1 plating, Table 3, and plating specifications of Table 2, for a 1.5% NaCl solution at 50°C.

Table 4. Electrochemical parameters of specimens in 1.5% NaCl solution attained from the polarization test..

β_c(mV/decade)	β_a(mV/decade)	R_p(KΩ.cm^2)	E_{cor}(mV)	I_{cor}(μA.cm^{-2})	Sample
24.285	59.741	250	-580-	0.03	Range-1
25.031	58.170	1.68	-520	4.8	SS.316L

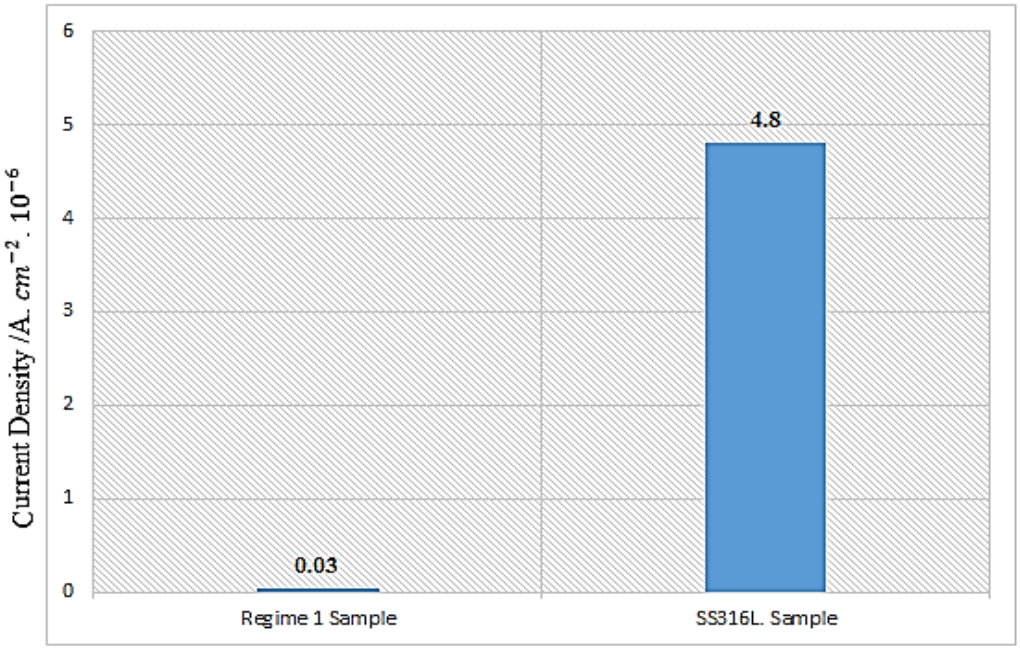

Fig. 7. Comparison between the polarization test results in 1.5% NaCl solution at 50°C from the plated sample under range-1 and bare SS316L.

High corrosion resistance results from Cr-dopped nickel matrix using reverse pulse frequencies with La. It has a pronounced effect on the structure at less than 1g.L^{-1} concentration by enhancing the nucleation

process so that it creates a coherent chloride-resistant structure. Lanthanum dissolves as La^{+3} cations (with their electronic structures) are favorably adsorbed on the surface of the cathode. It disturbs the positive charge balance of the catholyte, which is rebalanced by more Ni^{+2} migration. In fact, the initial adsorption of La^{+3} increases the cathodic current to facilitate the process of nickel ions reduction. The discharge of Ni^{+2} by employing reverse pulse range increases over-potential, which in turn enhances the nucleation of nickel grains. Finally, it results in a fine grain structure [31, 41]. As indicated by the linear scan results of Fig. 4, the amount of lanthanum taken up in the surface layer is very low due to its relatively low concentration in the bath and also its difficult deposition nature. Lanthanum sources like $LaCl_3.7H_2O$ and the reverse pulse condition provide optimal co-deposition to this element within the Ni matrix. The pulse electroplating with the possibility of reverse currents with varying frequency enables the controllability of discharge time and removal time of initial nuclei to achieve desired adhesion, as shown in Fig. 5(a). In fact, a cohesive and adhesive Ni coating with appropriate grain size and capable of forming Cr_2O_3 will exhibit the desired corrosion resistance properties. In contrast to the SS316L and other samples, it is demonstrated in the wide passive region formed in the range-1 sample polarization diagram (Fig. 6).

Excellent properties of lanthanum-dopped nickel coating can mainly be attributed to the three effects of rare-earth elements on the electrochemical depositing process: Firstly, the process of deposition is adsorbing the cation on the surface of a cathode. La is a surface-active element with a rather large atomic radius of 0.1877nm. La^{3+} is more easily adsorbed on the surface of a cathode due to the outer layer of lanthanum's electronic structure. When the plating process begins, Ni^{2+} is reduced on the surface of the cathode. However, La^{3+} does not participate in the reaction. The positive charge loss should be compensated by the new cations (La^{3+}, Ni^{2+}). Therefore, the Ni^{2+} content in the electric double layer decreases while the content of La^{3+} increases. It avoids the provisioning process and reduces Ni^{2+} in the bath. The schematic diagram of this process is demonstrated in Fig. 8. It requires a high over-potential to provide the energy of Ni^{2+} reduction, thus altering the deposition of Ni^{2+} and refining the grain size. Secondly, the over-potential also reduces the hydrogen evolution of Fig. 8, the schematic diagram of the cathode reaction, and the cathode surface. Therefore it reduces the hydrogen embrittlement and pinholes and makes perfect surface integrity. Thirdly, the outermost electronic structure of rare-earth lanthanum makes lanthanum ion adsorbed on the surface of the cathode. The cathodic potential needs to be increased to supply the Ni^{2+} energy reduction, increase the speed of the new crystal nuclei's formation, and then refine the grains [27, 28, 41].

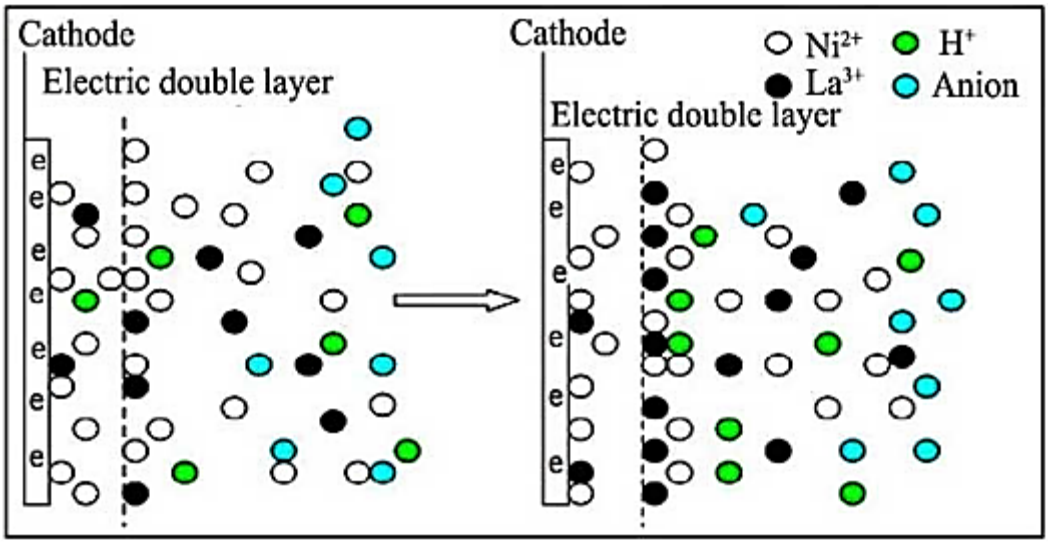

Fig. 8. Schematic diagram of the cathode reaction.

4. Conclusion

- Tertiary high entropy coatings composed of Ni-Fe-Cr-La with controlled metallurgical properties are coated on an SS316L substrate using a hybrid PRP electroplating technique and compounds of lanthanum as modifiers.
- Optimizing the Watts plating bath significantly improves the morphology and corrosion resistance properties of the resulting coating. This is performed by adding useful compounds of saccharin and SDS to increase the quality and fineness of the coating and use the combination of AlCl3 that leads to an increase in the electrical conductivity of the plating bath.

- The polarization test result indicated that the coated sample exhibits ~160 times lower corrosion current than the uncoated SS316L steel when attacked by chloride.
- The final result is a conversion coating with an adhesion due to the penetration zone. This penetration is due to the dissolution and redeposition of the substrate constituents during different phases of PRP electroplating.

References

[1] D. Krouse, N. Laycock, C. Padovani, "Modelling pitting corrosion of stainless steel in atmospheric exposures to chloride containing environments", Corrosion Engineering, Science and Technology, Vol. 49, No. 6, 2014, pp. 521-528.

[2] B. Lorsbach, E. Schmitz, "Influence of test parameters of potentiodynamic current density measurements on the determination of the pitting corrosion resistance of austenitic stainless steels", Materials and Corrosion, Vol. 69, No. 1, 2018, pp. 37-43.

[3] G. Bai, S. Lu, D. Li, Y. Li, "Influences of niobium and solution treatment temperature on pitting corrosion behaviour of stabilised austenitic stainless steels", Corrosion Science, Vol. 108, 2016, pp. 111-124.

[4] N.T Nga, T. Shinohara, T.H. Le, "Effects of Environment Factors on Stress Corrosion Cracking of Austenitic Stainless Steels in Atmospheric Environments", Zairyo-to-Kankyo, Vol. 66, No. 6, 2017, pp. 209-213.

[5] H.S Klapper, J. Stevens, G. Wiese, "Pitting Corrosion Resistance of CrMn Austenitic Stainless Steel in Simulated Drilling Conditions—Role of pH, Temperature, and Chloride Concentration", Corrosion, Vol. 69, No. 11, pp. 1095-1102.

[6] B. R. Tzaneva, M. H. Loukaycheva, L. B. Fachikov, L. Ts. Jekova, " Effect of chloride ions on corrosion behaviour of austenitic nickel and nickel free stainless steels in phosphoric acid solutions", Corrosion Engineering, Science and Technology, Vol. 50, No. 8, 2015, pp. 568-578.

[7] H.S Klapper, C. Menendez, S. Jesse, "Pitting Corrosion Resistance Influencing Corrosion Fatigue Behavior of an Austenitic Stainless Steel in Chloride-Containing Environments", Corrosion, Vol. 76, No. 4, 2020, pp. 398-410.

[8] R. Yamanoglu, E. Fazakas, F. Ahnia, D. Alontseva, F. Khoshnaw, "Pitting Corrosion behaviour of Austenitic Stainless-Steel Coated on $Ti_6A_{l4}V$ Alloy in Chloride Solutions", Advances in Materials Science, Vol. 21, No. 2, 2021, pp. 5-15.

[9] R. T. Loto, "Data on the Corrosion Resistance and Polarization Behaviour of Lean Austenitic and Ferritic Stainless Steels in Neutral Chloride Media", Oriental Journal of Chemistry, Vol. 35, No. 3, 2019, pp. 1138-1142.

[10] M.H. Jang, J.Y. Kang, J.H. Jang, T.H. Lee, C. Lee, "Hot deformation behavior and microstructural evolution of alumina-forming austenitic heat-resistant steels during hot compression", Materials Characterization, Vol. 123, 2017, pp. 207-217.

[11] D.B Park, S.M Hong, K.H Lee, M.Y Huh, J.Y Suh, S.C Lee, WS Jung, "High-temperature creep behavior and microstructural evolution of an $18Cr_9Ni_3CuNbVN$ austenitic stainless Steel", Materials Characterization, Vol. 93, 2014, pp. 52-61.

[12] L. Liu, S. Wu, Y. Chen, et al, "Oxidation behavior of RE-modified nickel-based superalloy between 952℃ and 1150℃ in air. Transactions of Nonferrous", Metals Society of China, Vol. 26, 2016, pp. 1163-1169.

[13] H.T Mallikarjuna, W.F Caley, N.L Richards, "Oxidation Kinetics and Oxide Scale Characterization of Nickel-Based Superalloy IN738LC at 900°C", Journal of Materials Engineering & Performance, Vol. 26, 2017, pp. 1-9.

[14] Z. Zheng, S. Wang, J. Long, J. Wang, K. Zheng, "Effect of Rare Earth Elements on High Temperature Oxidation Behavior of Austenitic Steel", Corrosion Science, Vol. 164, 2020, pp. 108-155.

[15] S. R. J Saunders, J. R. Nicholls, "Coatings and surface treatments for high temperature oxidation resistance", Metal Science Journal, Vol. 5, 2013, pp. 780-798.

[16] A. Karimi, R. Soltani, M. Ghambari, et al, "High temperature oxidation resistance of plasma sprayed and surface treated YSZ coating on Hastelloy X", Surface & Coatings Technology, Vol. 321, 2017, pp. 378-385.

[17] H. Liu, X. Zhang, Y. Jiang, et al, "Microstructure and high temperature oxidation resistance of in-situ synthesized TiN/Ti_3Al intermetallic composite coatings on Ti_6Al_4V alloy by laser cladding process", Journal of Alloys & Compounds, Vol. 670, 2016, pp. 268-274.

[18] W. Hansal, "Pulse plating as a core technology of surface finishing in the twenty-first century: review of the Eighth European Pulse Plating Seminar", Transactions of the IMF, Vol. 96, No. 3, 2018, pp. 115-117.

[19] J.-C. Puippe, "Unconventional pulse plating parameters for surface area measurement applications", Transactions of the IMF, Vol. 99, No. 1, 2021, pp. 17-22.

[20] C. Y. Chen, C. C. Hsu, U. W. Liu, C. A. Huang, "Characterization of Cr-Ni Multilayers from Chromium(III)-Nickel(II) Baths Using Pulse-Current Plating", ECS Transactions, Vol. 2, No. 3, 2019, pp. 413-418.

[21] J. Zhang, C. Su, X. Chen, H. Liu, L. Zhang, "First-principles study on pitting corrosion of Al deoxidation stainless steel with rare earth element (La) treatment", Materials Today Communications, Vol. 27, 2021, pp. 102-114.
[22] Y. C. Yu, S. H. Zhang, S. B. Wang, "Effects of Cerium on the Inclusions and Pitting Corrosion Behavior of 434 Ferritic Stainless Steel", High Temperature Materials and Processe, Vol. 37, No. 9, 2018, pp. 807-814.
[23] W. Zheng, X. Yan, S. Xiong, G. Wang, G. Li, "Pitting corrosion behavior of cerium treated HSLA steel induced by sulfide inclusions in 3.5 wt% NaCl solution", Journal of Rare Earths, Vol. 39, No. 3, 2021, pp. 348-356.
[24] N. Yin, C.L. Jing, H.B Li, R.S Chu, B. Chen, "Effect of Rare Earth Elements on the Inclusion Behavior in Low Alloy Structural Steel", Materials Science Forum, Vol. 944, 2019, pp. 364-372.
[25] X. Cheng, Z. Jiang, D. Wei, et al, "Characteristics of oxide scale formed on ferritic stainless steels in simulated reheating atmosphere", Surface & Coatings Technology, Vol. 258, 2014, pp. 257-267.
[26] Q. Wang, Q. Yao, Y. Wang, et al, "Research on the oxidation behavior of novel γ/γ'-strengthened Co-9Al-10W alloys combined with chromium and rare earth elements", Journal of Materials Research, Vol. 31, 2016, pp. 3332-3344.
[27] X. Xing, H. Wang, P. Lu, Z. Han, "Influence of rare earths on electrochemical corrosion and wear resistance of RE–Cr/Ti pack coatings on cemented 304 stainless steel", Surface And Coating Technology, Vol. 291, 2016, pp. 151-160.
[28] C. Liu, R.I Revilla, Z. Liu, D. Zhang, X. Li, H. Terryn, "Effect of inclusions modified by rare earth elements (Ce, La) on localized marine corrosion in Q460NH weathering steel", Corrosion Science, Vol. 129, 2017, pp. 82-90.
[29] D. Xueliang, W. Deren, Z. Yangqing, " Effect of mechanical attrition on microstructure and properties of electro-deposition coatings on NdFeB", Journal of Rare Earths, Vol. 32, No. 9, 2014, pp. 867-873.
[30] J. Guo, L. Bingwen, H. Dingding, C. Xiufang, et al, "Influence of rare earths addition on residual stress of Fe-based coating prepared by brush plating technology", Journal of Rare Earths, Vol. 34, 2016, pp. 336-345.
[31] M.A.M. Ibrahim, R.S. Bakdash, "New non-cyanide acidic copper electroplating bath based on glutamate complexing agent", Surface Coating Technology, Vol. 282, 2015, pp. 139–148.
[32] Brian Hinderliter, "Response of Electrochemical Impedance Spectroscopy to Evolving Coating Systems", ECS. Transactions, Vol. 41, No. 15, 2019, pp. 39-51.
[33] N. Imaz, M. Ostra, M. Vidal, J.A. Díez, M. Sarret, E. García-Lecina, "Corrosion behaviour of chromium coatings obtained by direct and reverse pulse plating electrodeposition in NaCl aqueous solution", Corrosion Science, Vol. 78, 2014, pp. 251-259.
[34] M.S. Chandrasekar, Malathy Pushpavanam, "Pulse and pulse reverse plating—Conceptual, advantages and applications", Electrochimica Acta, Vol. 53, No. 8, 2008, pp. 3313-3322.
[35] G. Wang, D. Li, Y. Zuo, Y. Tang, X. Zhang, X. Zhao, "The Improvement of Hardness and Corrosion Resistance of Electroplated Pd-Ni Film on 316L Stainless Steel by $CeCl_3$", Coatings, Vol. 10, No. 2, 2020, pp. 161-171.
[36] R. Gupta, A. Sharma, U. Pandel, L. Ratke, "Effect of stirring speed on microstructure of A356 alloy cast through rheometal process", International Journal of Materials Research, Vol. 108, No. 8, 2017, pp. 648-655.
[37] P. Marcolin, M. Longhi, L. P. Zini, B. Proença, et al, " Influence of the pH and Stirring Speed of the Electrodeposition Bath in the Performance of Zinc and Zinc-Nanocomposite Coatings", Materials Science Forum, Vol. 899, 2017, pp. 283-288.
[38] S. An, Y.I Kim, H.S Jo, M.W Kim, M.W Lee, A.L Yarin, et al, "Silver-decorated and palladium-coated copper electroplated fibers derived from electrospun polymer nanofibers", Chem. Eng. J., Vol. 327, 2017, pp. 336–342.
[39] Y. Kamimoto, S. Okura, T. Hagio, T. Wada, H. Tanaka, et al, "Nickel–carbon composite plating using a Watts nickel electroplating bath. SN Applied Sciences", Vol. 2, No. 2, 2020, pp. 1-6.
[40] M. Mohammadi, M. Ghorbani, "Wear and corrosion proper- ties of electroless nickel composite coatings with PTFE and/or MoS2 particles", J. Coat Technol Res, Vol. 8, 2011, pp. 527–533
[41] W. Dan, Y. Cheng, J. Huiming, J. Zhang, J. Gao, "Influence of LaCl3 addition on microstructure and properties of nickel-electroplating coating", Journal of Rare Earths, Vol. 31, No. 2, 2013, pp. 209-214.